Hepatic G_i signaling regulates whole-body glucose homeostasis

Mario Rossi,[1] Lu Zhu,[1] Sara M. McMillin,[1] Sai Prasad Pydi,[1] Shanu Jain,[1] Lei Wang,[1] Yinghong Cui,[1] Regina J. Lee,[1] Amanda H. Cohen,[1] Hideaki Kaneto,[2] Morris J. Birnbaum,[3] Yanling Ma,[4] Yaron Rotman,[4] Jie Liu,[5] Travis J. Cyphert,[6] Toren Finkel,[5] Owen P. McGuinness,[6] and Jürgen Wess[1]

[1]Molecular Signaling Section, Laboratory of Bioorganic Chemistry, National Institute of Diabetes and Digestive and Kidney Diseases (NIDDK), Bethesda, Maryland, USA. [2]Osaka University Graduate School of Medicine, Osaka, Japan. [3]Cardiovascular and Metabolic Diseases (CVMED), Pfizer Inc., Cambridge, Massachusetts, USA. [4]Liver and Energy Metabolism Unit, Liver Diseases Branch, NIDDK, Bethesda, Maryland, USA. [5]Center for Molecular Medicine, National Heart, Lung, and Blood Institute (NHLBI), Bethesda, Maryland, USA. [6]Departments of Molecular Physiology and Biophysics, Vanderbilt University Medical Center, Nashville, Tennessee, USA.

An increase in hepatic glucose production (HGP) is a key feature of type 2 diabetes. Excessive signaling through hepatic G_s–linked glucagon receptors critically contributes to pathologically elevated HGP. Here, we tested the hypothesis that this metabolic impairment can be counteracted by enhancing hepatic G_i signaling. Specifically, we used a chemogenetic approach to selectively activate G_i-type G proteins in mouse hepatocytes in vivo. Unexpectedly, activation of hepatic G_i signaling triggered a pronounced increase in HGP and severely impaired glucose homeostasis. Moreover, increased G_i signaling stimulated glucose release in human hepatocytes. A lack of functional G_i-type G proteins in hepatocytes reduced blood glucose levels and protected mice against the metabolic deficits caused by the consumption of a high-fat diet. Additionally, we delineated a signaling cascade that links hepatic G_i signaling to ROS production, JNK activation, and a subsequent increase in HGP. Taken together, our data support the concept that drugs able to block hepatic G_i–coupled GPCRs may prove beneficial as antidiabetic drugs.

Introduction

Type 2 diabetes (T2D) has emerged as a major health problem worldwide (1). In addition to other pathophysiological features, T2D is characterized by an increase in hepatic glucose production (HGP) (2–4). Some antidiabetic drugs, such as metformin, exert their therapeutic actions by inhibiting HGP increases (3). To stimulate the development of novel therapeutic agents that target pathologically elevated HGP, it is critical to gain a better understanding of the molecular pathways that regulate hepatic glucose fluxes.

Hepatocyte function is regulated by the activity of cell-surface receptors that belong to the superfamily of GPCRs (5). In general, GPCRs are linked to distinct families of heterotrimeric G proteins (primarily G_s, G_i, and G_q; representative GPCRs: glucagon, α_2-adrenergic, and α_1-adrenergic receptors, respectively). The important metabolic roles of hepatic glucagon receptors in maintaining normoglycemia under fasting conditions and in raising blood glucose levels in response to hypoglycemia are well recognized (6–8). The glucagon receptor (GCGR), which is abundantly expressed in hepatocytes, is linked to the stimulatory G protein G_s, which in turn activates adenylyl cyclase to promote the generation of cAMP (6, 9). This signaling pathway ultimately stimulates both glycogenolysis and gluconeogenesis (6), leading to a pronounced increase in HGP. Interestingly, glucagon levels are inappropriately elevated in patients suffering from T2D, suggesting that increased signaling through hepatic GCGRs may play a central role in the pathophysiology of T2D (4, 8).

In most tissues or cell types, the ability of G_s-coupled receptors to stimulate adenylyl cyclase is counteracted by the activity of GPCRs that are linked to G proteins of the G_i family that directly inhibit adenylyl cyclase function (10). Hepatocytes express a number of G_i-coupled receptors including the α_2-adrenergic (11) and CB_1 cannabinoid receptors (12, 13). We therefore hypothesized that receptor-mediated activation of hepatocyte G_i signaling pathways might prove useful in reducing the exaggerated hepatic GCGR activity that is characteristic of T2D. However, like virtually all other GPCRs, hepatic G_i–linked receptors are also expressed in many other tissues and cell types (14). For this reason, it is impossible to assess the in vivo roles of hepatic G_i–coupled receptors by simply administering receptor subtype–selective agonists or antagonists.

To circumvent these difficulties, we used a chemogenetic strategy that involves the use of a designer GPCR (designer receptor exclusively activated by a designer drug [DREADD]) that is selectively linked to G_i-type G proteins (15, 16). This designer GPCR (known as hM4Di and referred to herein as Di) represents a mutant M_4 muscarinic receptor that no longer binds its endogenous agonist, acetylcholine, but can be selectively activated by clozapine-*N*-oxide (CNO), a compound that

▶ Related Commentary: p. 567

Authorship note: M. Rossi and L. Zhu contributed equally to this work.
Conflict of interest: The authors have declared that no conflict of interest exists.
Submitted: April 10, 2017; **Accepted:** November 17, 2017.
Reference information: *J Clin Invest*. 2018;128(2):746–759.
https://doi.org/10.1172/JCI94505.

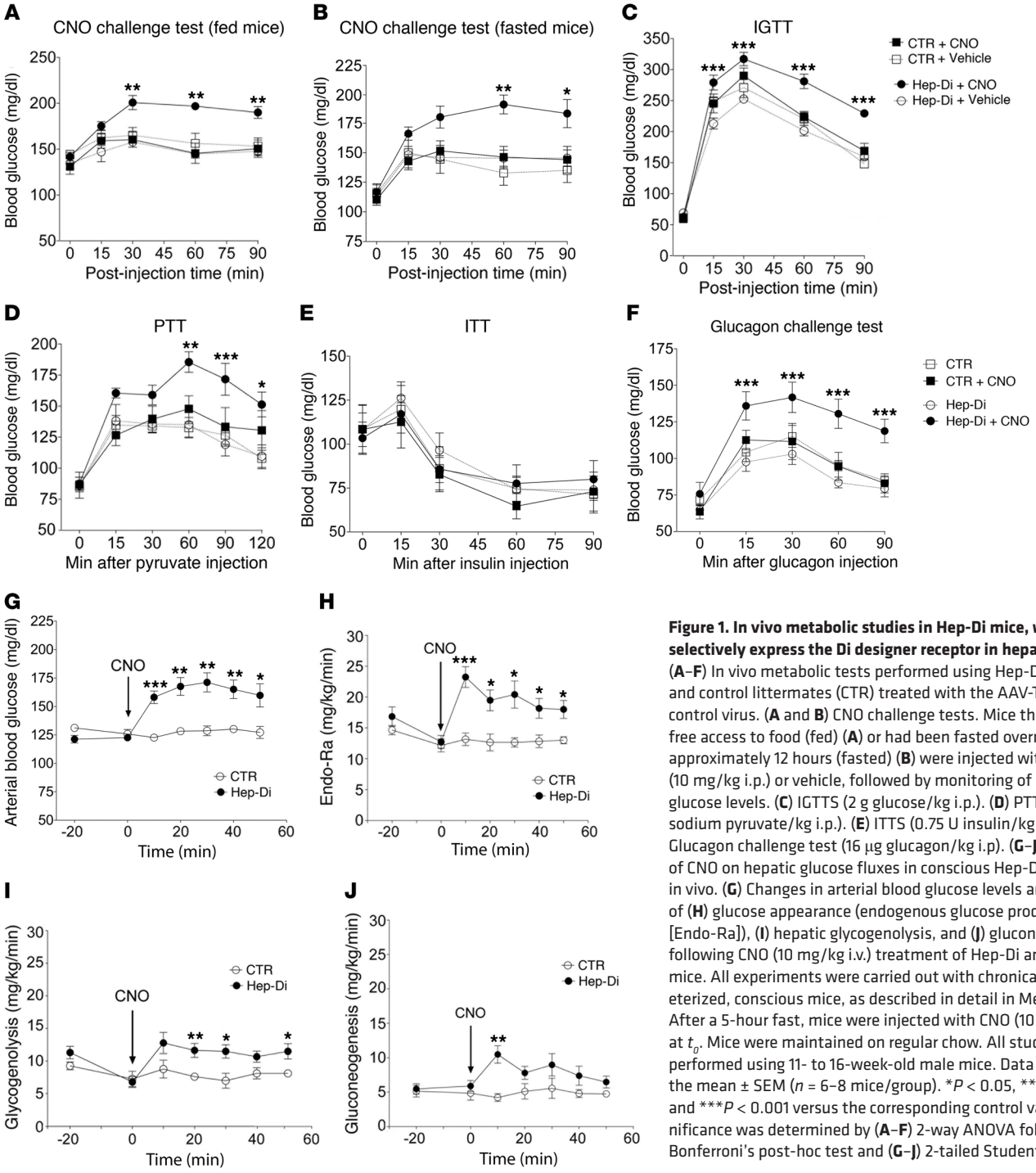

Figure 1. In vivo metabolic studies in Hep-Di mice, which selectively express the Di designer receptor in hepatocytes. (**A**–**F**) In vivo metabolic tests performed using Hep-Di mice and control littermates (CTR) treated with the AAV-TBG-EGFP control virus. (**A** and **B**) CNO challenge tests. Mice that had free access to food (fed) (**A**) or had been fasted overnight for approximately 12 hours (fasted) (**B**) were injected with CNO (10 mg/kg i.p.) or vehicle, followed by monitoring of blood glucose levels. (**C**) IGTTS (2 g glucose/kg i.p.). (**D**) PTT (2 g sodium pyruvate/kg i.p.). (**E**) ITTS (0.75 U insulin/kg i.p.). (**F**) Glucagon challenge test (16 μg glucagon/kg i.p). (**G**–**J**) Effect of CNO on hepatic glucose fluxes in conscious Hep-Di mice in vivo. (**G**) Changes in arterial blood glucose levels and rates of (**H**) glucose appearance (endogenous glucose production [Endo-Ra]), (**I**) hepatic glycogenolysis, and (**J**) gluconeogenesis following CNO (10 mg/kg i.v.) treatment of Hep-Di and control mice. All experiments were carried out with chronically catheterized, conscious mice, as described in detail in Methods. After a 5-hour fast, mice were injected with CNO (10 mg/kg) at t_0. Mice were maintained on regular chow. All studies were performed using 11- to 16-week-old male mice. Data represent the mean ± SEM (n = 6–8 mice/group). $^*P < 0.05$, $^{**}P < 0.01$, and $^{***}P < 0.001$ versus the corresponding control value. Significance was determined by (**A**–**F**) 2-way ANOVA followed by Bonferroni's post-hoc test and (**G**–**J**) 2-tailed Student's t test.

is otherwise pharmacologically inert (15, 16). We demonstrate that activation of G_i-type G proteins in hepatocytes greatly enhances HGP, resulting in a profound impairment in glucose homeostasis. In contrast, mice lacking functional G_i in hepatocytes show the opposite phenotype and are protected against obesity-associated deficits in glucose homeostasis. We also delineate a ROS-dependent pathway through which hepatocyte G_i signaling stimulates glucose output from the liver. These surprising new findings could pave the way for the development of novel antidiabetic drugs.

Results

Generation of mice expressing the G_i DREADD Di in hepatocytes. To achieve selective expression of Di in hepatocytes, we injected 8-week-old WT male mice (C57BL/6 strain; Taconic) with an adeno-associated virus (AAV) coding for the Di designer receptor (AAV-TBG-Di; 1×10^{11} infectious particles/mouse) via the tail vein. Quantitative reverse transcription PCR (qRT-PCR) studies demonstrated that this procedure resulted in a liver-specific expression of Di (Supplemental Figure 1A; supplemental material available online with this article; https://doi.org/10.1172/JCI94505DS1)

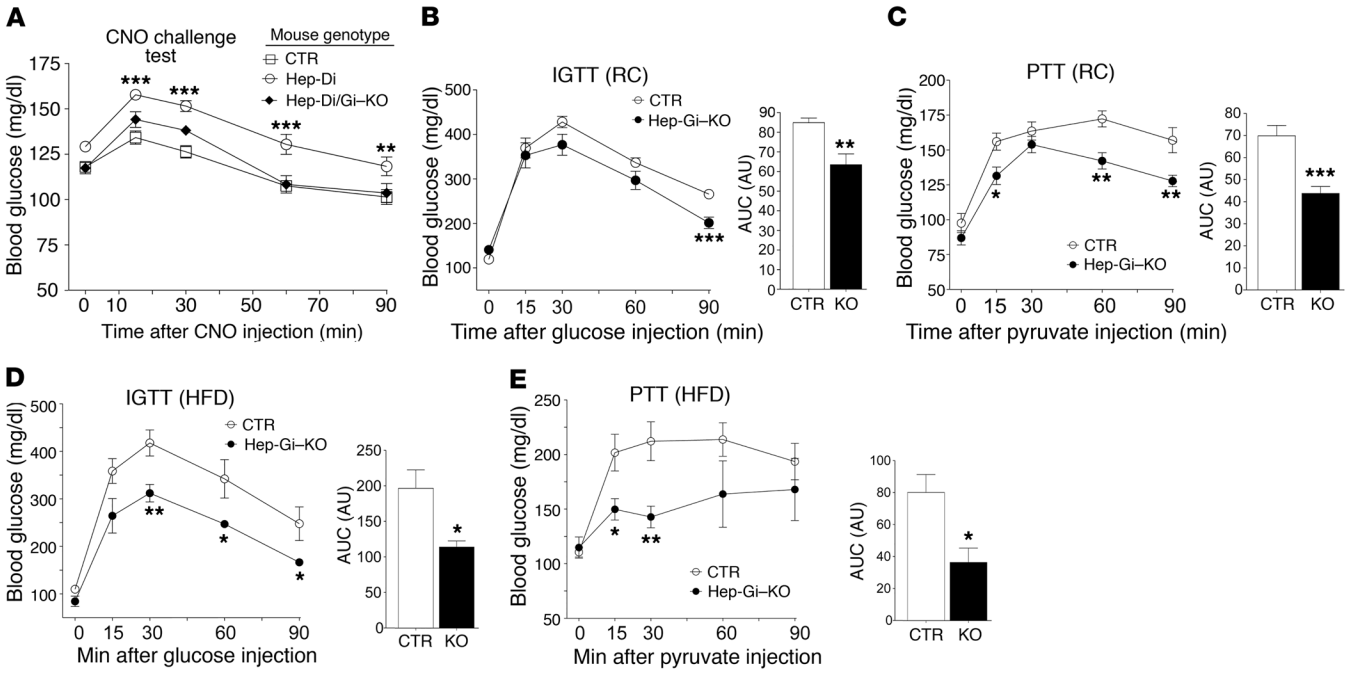

Figure 2. In vivo metabolic studies in mice Hep-Go–KO mice, which lack functional G_i-type G proteins in hepatocytes. (**A**) CNO-induced increases in blood glucose levels in Hep-Di mice required functionally intact hepatic G_i. Mice of the indicated genotypes were fasted for 4 hours, followed by an i.p. injection of CNO (10 mg/kg) and monitoring of blood glucose levels. Studies were conducted using 12-week-old female mice consuming regular chow (RC). (**B** and **D**) IGTTs. Hep-Gi–KO mice and their control littermates were maintained on either RC (**B**) or a HFD (RC, 2 g glucose/kg; HFD, 1 g glucose/kg) (**D**). (**C** and **E**). PTTs (2 g sodium pyruvate/kg i.p.). Mice of the indicated genotypes were maintained on either RC (**C**) or a HFD (**E**). IGTTs and PTTs were performed in male mice that were at least 14 weeks old. Data represent the mean ± SEM (RC, n = 9 or 10 mice/group; HFD, n = 5 or 6 mice/group). $^*P < 0.05$, $^{**}P < 0.01$, and $^{***}P < 0.001$, compared with the corresponding control group. Statistical significance was determined by (**A**) 1-way ANOVA followed by Bonferroni's post-hoc test and (**B**–**E**) 2-tailed Student's t test.

that was maintained at comparable levels for at least 3 months. To monitor actual Di receptor densities, we performed [^{3}H]-*N*-methylscopolamine ([^{3}H]-NMS; NMS is a muscarinic antagonist) saturation binding studies using liver membranes prepared 2 weeks after treatment of mice with the AAV-TBG-Di virus (note that [^{3}H]-NMS retains the ability to bind to DREADDs with high affinity; ref. 17). This analysis showed that Di was expressed at a density of 104 ± 34 fmol/mg liver membrane protein (Supplemental Figure 1B; n = 3). This receptor density is within the expression range of endogenous GPCRs expressed by peripheral or central tissues. Here, we refer to the mice injected with the AAV-TBG-Di virus simply as Hep-Di mice. For control purposes, we also injected C57BL/6 WT mice (Taconic) with a pharmacologically inert AAV coding for EGFP (AAV-TBG-EGFP) (control mice). No specific [^{3}H]-NMS binding sites were detectable in liver membranes from control mice (0.44 ± 0.46 fmol/mg; n = 3). We initiated mouse phenotyping studies 2 weeks after AAV treatment.

Functional studies with Di-expressing hepatocytes. We first subjected primary hepatocytes prepared from Hep-Di and control mice to various signaling assays. As expected for a G_i-coupled receptor, CNO treatment (10 μM) of Hep-Di hepatocytes led to a strong reduction in glucagon-induced cAMP production (Supplemental Figure 2A). In contrast, CNO did not affect glucagon-induced cAMP accumulation in control hepatocytes (Supplemental Figure 2B). CNO treatment (10 μM) of Hep-Di hepatocytes had no significant effect on intracellular calcium levels ($[Ca^{2+}]_i$), which is typical for most G_i-coupled receptors (Supplemental Figure 2C). However, Hep-Di hepatocytes responded normally to arginine vasopressin (AVP), which triggers increases in $[Ca^{2+}]_i$ by activating endogenous G_q-coupled V_1 vasopressin receptors (18) (Supplemental Figure 2C). These data demonstrated that the Di designer receptor had the predicted signaling profile when expressed in mouse hepatocytes.

In vivo metabolic studies with Hep-Di and control mice. We next subjected Hep-Di and control mice to a series of in vivo metabolic tests. Strikingly, treatment of Hep-Di mice with a single dose of CNO (10 mg/kg i.p.) led to a pronounced increase in blood glucose levels, in both mice that had free access to food and those that had been fasted overnight for approximately 12 hours (Figure 1, A and B). We did not observe this effect in saline-treated Hep-Di mice or in control mice that had received either saline or CNO (Figure 1, A and B).

In an i.p. glucose tolerance test (IGTT), we found that CNO treatment (10 mg/kg i.p.) of control mice had no significant effect on blood glucose excursions as compared with saline-injected control or Hep-Di mice (Figure 1C). On the other hand, CNO administration led to a significant impairment in glucose tolerance in Hep-Di mice (Figure 1C). These CNO-induced deficits in glucose tolerance were not due to changes in glucose-induced insulin secretion (Supplemental Figure 3). We obtained similar results when we performed a pyruvate challenge test, which is commonly used to study gluconeogenesis in vivo. Combined treatment of Hep-Di mice with sodium pyruvate (2 g/kg i.p.) and CNO (10 mg/kg i.p.) led to greatly

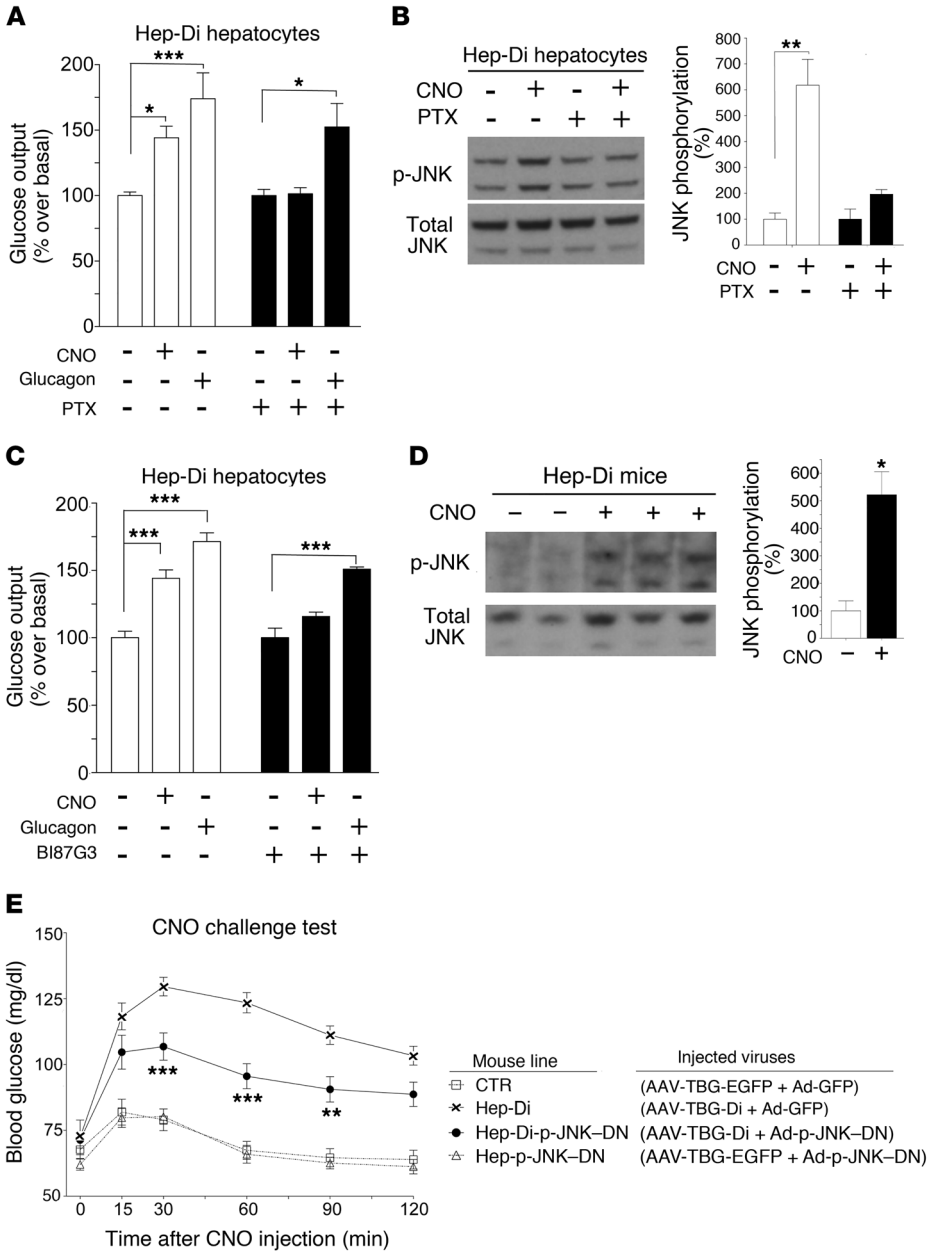

Figure 3. Key role of JNK in mediating the metabolic effects of hepatic Di signaling. (**A** and **C**) Glucose output assays with primary Hep-Di hepatocytes. The ability of CNO (10 μM) and glucagon (100 nM) to stimulate glucose release from primary Hep-Di hepatocytes was examined. Experiments were performed with or without PTX (300 ng/ml) (**A**), or with or without BI87G3 (10 μM) (**C**), a selective JNK inhibitor. In vitro glucose output data represent the mean ± SEM from 3 independent experiments. (**B** and **D**) Activation of hepatic Di signaling promoted JNK phosphorylation. (**B**) In vitro studies. Primary Hep-Di hepatocytes were cultured in the presence or absence of PTX (300 ng/ml). Cells were incubated with CNO (10 μM) for 15 minutes at 37°C, followed by Western blot analysis of cell lysates. (**D**) In vivo studies. Hep-Di mice that had been fasted overnight received a single injection of CNO (10 mg/kg i.p.) or vehicle (–). Liver tissue was collected 15 minutes later, and liver lysates were subjected to Western blotting. p-JNK expression levels were normalized to total JNK expression. Immunoreactive bands were quantified using ImageJ software (NIH). The quantitative data shown in **B** and **D** represent the mean ± SEM from 3 independent experiments. (**E**) CNO challenge test. After an overnight fast, mice treated with the indicated viruses received a single injection of CNO (10 mg/kg i.p.) followed by monitoring of blood glucose levels. Data represent the mean ± SEM (n = 9–10 male mice/group). *P < 0.05, **P < 0.01, and ***P < 0.001, compared with the corresponding control group. Statistical significance was determined by (**A**, **B**, **C**, and **E**) 2-way ANOVA followed by Bonferroni's post-hoc test and (**D**) 2-tailed Student's t test. See complete unedited blots in the supplemental material.

enhanced blood glucose excursions as compared with glucose responses observed in Hep-Di mice treated with pyruvate alone (Figure 1D). As expected, no CNO effect was detectable in control mice (Figure 1D). These observations suggest that activation of hepatic Di (G_i) signaling leads to a robust stimulation of glucose output in vivo. An i.p. insulin tolerance test (ITT) indicated that peripheral insulin sensitivity remained unchanged in CNO-treated Hep-Di mice (Figure 1E).

To examine whether Di activation in hepatocytes modulated the hepatic actions of glucagon in vivo, we performed a glucagon challenge test. Strikingly, we observed that coinjection of CNO (10 mg/kg i.p.) with glucagon (16 μg/kg i.p.) greatly enhanced the hyperglycemic effects of glucagon in Hep-Di mice, but not in control mice (Figure 1F). This finding supports the surprising concept that activation of hepatic G_i signaling enhances HGP, in contrast to our initial hypothesis.

We next examined whether the Di-mediated increases in blood glucose levels were dependent on intact glucagon signaling. To address this question, we treated Hep-Di and control mice with the anti-GCGR antibody mAB7.v44 (10 mg/kg i.p.) (19) 24 hours prior to CNO or glucagon injections. Control experiments showed that pretreatment of Hep-Di mice with the anti-GCGR antibody completely abolished glucagon-induced (16 μg/kg i.p.) hyperglycemic effects (Supplemental Figure 4A). On the other hand, administration of the anti-GCGR antibody had little or no effect on CNO-mediated (10 mg/kg i.p.) increases in blood glucose levels in Hep-Di mice (Supplemental Figure 4B). These data clearly indicate that Di signaling stimulates hepatic glucose release in a glucagon/GCGR-independent fashion.

Quantification of hepatic glucose fluxes in Hep-Di mice. In order to quantify hepatic glucose fluxes, we conducted isotope labeling studies using chronically catheterized, conscious Hep-Di mice

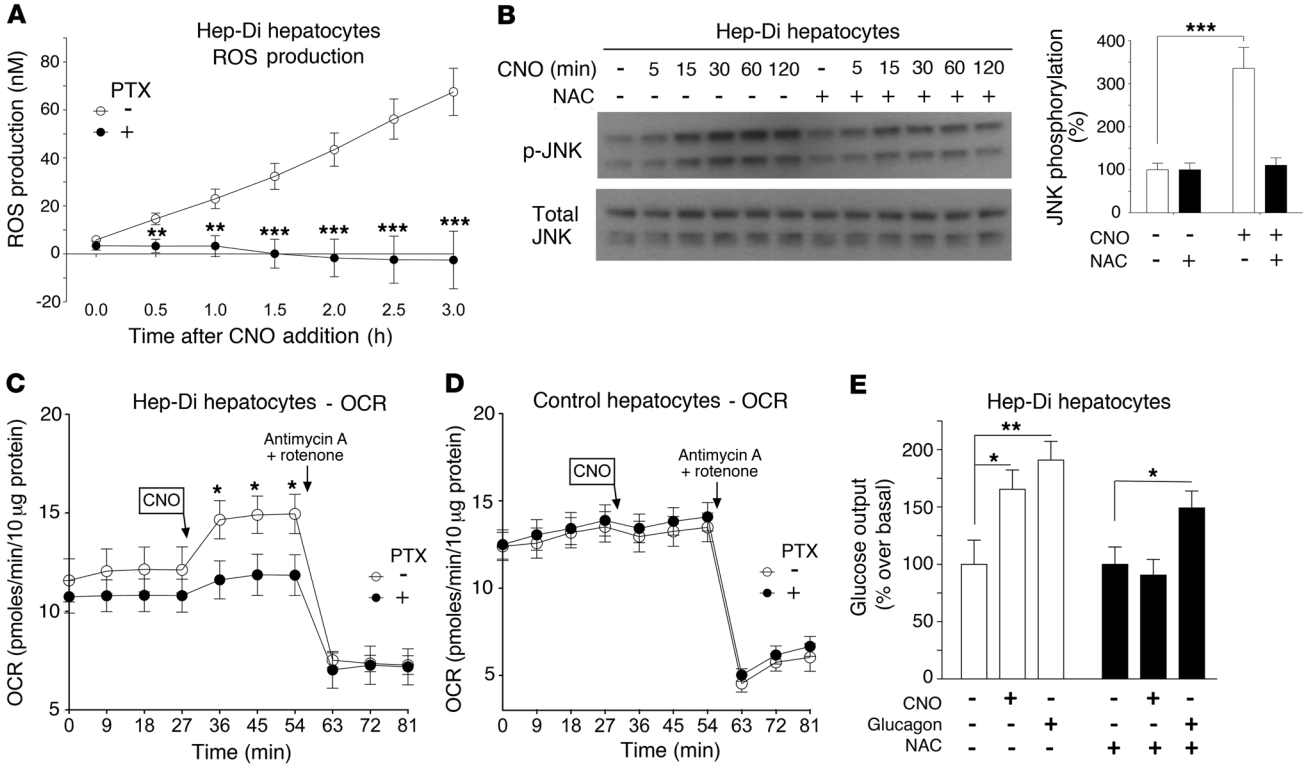

Figure 4. Hepatic Di signaling increases ROS production, JNK phosphorylation, and OCR. (**A**–**C** and **E**) Studies using Hep-Di hepatocytes. (**D**) Studies using control hepatocytes. (**A**) Enhanced ROS production caused by hepatocyte Di signaling was PTX sensitive. CNO (10 μM) treatment of Hep-Di hepatocytes led to time-dependent increases in ROS production. These responses were completely abolished in the presence of PTX (300 ng/ml). Data represent the mean ± SEM from 3 independent experiments. (**B**) Increased p-JNK caused by hepatocyte Di signaling was NAC sensitive. Primary hepatocytes from Hep-Di mice were incubated with CNO (10 μM) for the indicated durations at 37°C, followed by Western blot analysis of cell lysates. Incubations were done with or without the ROS scavenger NAC (5 mM). Representative immunoblots are shown. Quantitative data represent the mean ± SEM from 7 independent experiments (CNO incubation time: 15 min). p-JNK expression levels were normalized to total JNK expression. (**C** and **D**) Measurement of the OCR of primary mouse hepatocytes. CNO (10 μM) treatment of Hep-Di hepatocytes (**C**) caused a marked increase in the OCR. These effects were almost abolished in the presence of PTX (300 ng/ml). The mitochondrial inhibitors antimycin A and rotenone demonstrated that the increased OCR derived from mitochondrial metabolism. CNO had no significant effect on the OCR in control hepatocytes (**D**). The curves shown are representative of 3 independent experiments. The OCR was measured using Seahorse technology. (**E**) Glucose output assays were performed with primary Hep-Di hepatocytes. The ability of CNO (10 μM) and glucagon (100 nM) to stimulate glucose release from primary Hep-Di hepatocytes was examined. Experiments were done with or without NAC (5 mM). Data represent the mean ± SEM from 7 (**B**) or 3 (**A** and **E**) independent experiments. $*P < 0.05$, $**P < 0.01$, and $***P < 0.001$, compared with the corresponding control group. Statistical significance was determined by (**B** and **E**) 2-way ANOVA followed by Bonferroni's post-hoc test and (**A**, **C**, and **D**) 2-tailed Student's *t* test. See complete unedited blots in the supplemental material.

(see Methods) (20–22). After fasting the mice for 5 hours, [6,6-^{2}H] glucose was infused continuously into the jugular vein used to measure the rate of glucose appearance (Ra). Total body water was enriched with D_2O, from which the contribution of gluconeogenesis and glycogenolysis to Ra was estimated (23). After assessment of baseline glucose enrichment, the Hep-Di and control mice received a bolus of CNO (10 mg/kg i.v.). CNO treatment of Hep-Di mice, but not control mice, led to a rapid and sustained increase in arterial glucose concentrations and Ra (Figure 1, G and H). The CNO-mediated increase in Ra (Figure 1H) was due to significant and sustained increases in the rates of both glycogenolysis and gluconeogenesis (Figure 1, I and J).

In vivo metabolic studies in mice lacking functional G_i in hepatocytes. The metabolic phenotypes of the CNO-treated Hep-Di mice suggested that inhibition of hepatic G_i signaling might prove useful to reduce pathologically enhanced HGP. To explore this possibility, we generated mutant mice that lacked functional G_i-type G proteins selectively in hepatocytes. These mice were obtained by injecting an AAV coding for Cre recombinase (AAV-TBG-CRE) into the tail vein of *ROSA26^{PTX}* mice (24). In this latter mouse strain, the coding sequence of the S1 catalytic subunit of pertussis toxin (S1-PTX) is preceded by a floxed silencer cassette (24) (note that PTX leads to the functional inactivation of G_i-type G proteins via ADP ribosylation). This strategy led to the selective expression of S1-PTX in hepatocytes (Supplemental Figure 5A). For the sake of simplicity, we refer here to these mice simply as Hep-Gi–KO mice. The livers from Hep-Gi–KO mice appeared histologically normal and showed no signs of hepatotoxicity (data not shown).

Importantly, we found that the ability of CNO (10 mg/kg i.p.) to induce pronounced hyperglycemic effects was greatly diminished in Hep-Gi–KO mice expressing Di in a hepatocyte-specific fashion (Hep-Di/Gi–KO mice; Figure 2A). This observation indicates that the in vivo metabolic impairments caused by Di signaling in hepatocytes are indeed dependent on the activation of G_i-type G proteins.

IGTTs and pyruvate tolerance tests (PTTs) also showed that Hep-Gi–KO mice had significantly reduced blood glucose excur-

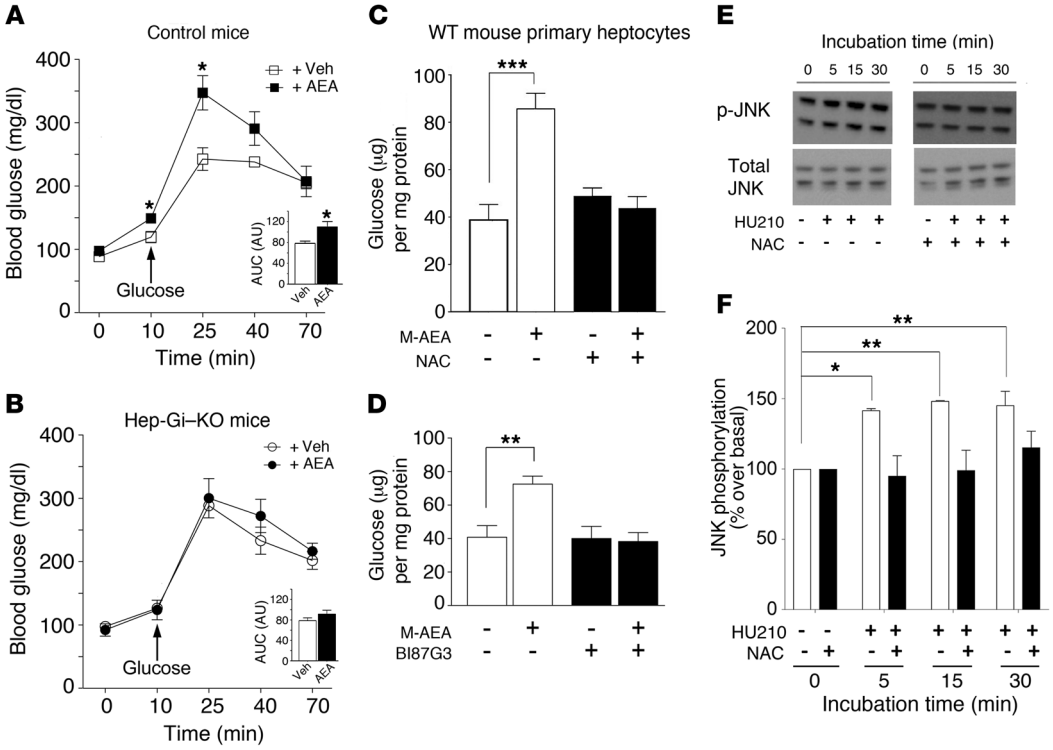

Figure 5. In vivo and in vitro studies with CB_1 cannabinoid receptor agonists. (**A** and **B**) IGTTs in control and Hep-Gi–KO mice. Note that AEA caused impaired glucose tolerance in control mice (**A**) but not in Hep-Gi–KO mice (**B**). Mice were fasted overnight for approximately 12 hours. Ten minutes before glucose injections (2 g/kg i.p.), mice were injected with either AEA (10 mg/kg i.p.) or vehicle (Veh). Studies were performed with female mice (at least 16 weeks of age). Data represent the mean ± SEM (n = 4 or 5 mice/group). *P < 0.05, compared with the vehicle-treated group. Statistical significance was determined by Student's t test. (**C**–**F**) Stimulation of WT mouse primary hepatocytes with CB_1 receptor agonists. Hepatocytes were prepared from male WT mice (~14 weeks of age) maintained on a HFD to boost CB_1 receptor expression levels (13). (**C** and **D**) Treatment of WT mouse hepatocytes with M-AEA (150 nM), a metabolically stable CB_1 receptor agonist. The agonist-induced increase in glucose output was completely absent in the presence of the ROS scavenger NAC (5 mM) or the selective JNK inhibitor BI87G3 (10 μM). (**E** and **F**) Incubation of WT mouse hepatocytes with HU210, a CB_1 receptor agonist. Hepatocytes were pretreated with NAC (5 mM) for 2 hours and then stimulated with HU210 (1 μM) for the indicated durations. Subsequently, p-JNK and total JNK expression levels were determined by Western blotting. (**E**) Representative Western blot. (**F**) Quantification of Western blot data. Immunoreactive bands were quantified using ImageJ. p-JNK expression levels were normalized to total JNK expression. Data represent the mean ± SEM from 3 independent experiments. *P < 0.05, **P < 0.01, and ***P < 0.001, compared with the corresponding control value. Statistical significance was determined by (**A** and **B**) 2-tailed Student's t test and (**C**, **D**, and **F**) 2-way ANOVA followed by Bonferroni's post-hoc test). See complete unedited blots in the supplemental material.

sions as compared with control littermates injected with the AAV-TBG-GFP virus (Figure 2, B–E). We observed that these effects were independent of the type of diet that the mice consumed (regular chow or a high-fat diet [HFD]). Importantly, in the HFD feeding studies, the metabolic deficits observed with control mice (glucose intolerance and enhanced in vivo gluconeogenesis) were absent in the Hep-Gi–KO mice (Figure 2, D and E). Body weights and blood glucose and plasma insulin levels were not significantly different between the HFD Hep-Gi–KO and HFD control mice (Supplemental Figure 5B).

Glucose output studies with primary Hep-Di hepatocytes. To confirm that the Di-mediated impairments in glucose homeostasis observed in vivo were indeed caused by altered hepatic glucose fluxes, we performed studies using primary hepatocytes isolated from Hep-Di mice (Hep-Di hepatocytes). We treated Hep-Di hepatocytes with either glucagon (100 nM), as a positive control, or CNO (10 μM), either in the absence or presence of PTX (300 ng/ml). We found that CNO treatment of Hep-Di hepatocytes stimulated glucose output in a fashion similar to that seen with glucagon (Figure 3A). Importantly, the stimulatory effect of CNO, but not that of glucagon, was completely abolished in the presence of PTX (Figure 3A). These observations strongly support the concept that Di-mediated stimulation of HGP depends on the activation of G_i-type G proteins.

ERK activation does not contribute to Di-stimulated HGP. Many studies have shown that G_i-coupled receptors can stimulate different MAPK signaling pathways, including the ERK and JNK signaling cascades (25–28). Given the important roles of activated MAPKs in regulating HGP (29–33), we hypothesized that MAPK-dependent signaling might contribute to the Di-mediated changes in hepatic glucose fluxes. Initially, we demonstrated that CNO (10 μM) treatment of Hep-Di hepatocytes led to a significant stimulation of ERK1/2 phosphorylation (Supplemental Figure 6, A and B). This effect was abolished in the presence of PTX (300 ng/ml) (Supplemental Figure 6, A and B), which is indicative of the involvement of G_i-type G proteins. To test the hypothesis that increased ERK1/2 phosphorylation was required for Di-mediated increases in HGP, we performed glucose output assays using isolated Hep-Di hepatocytes. Pretreatment with U0126 (10 μM), a selective MEK inhibitor that prevents ERK1/2 phosphorylation, did not impair the ability of CNO (10 μM) or glucagon (100 nM) to

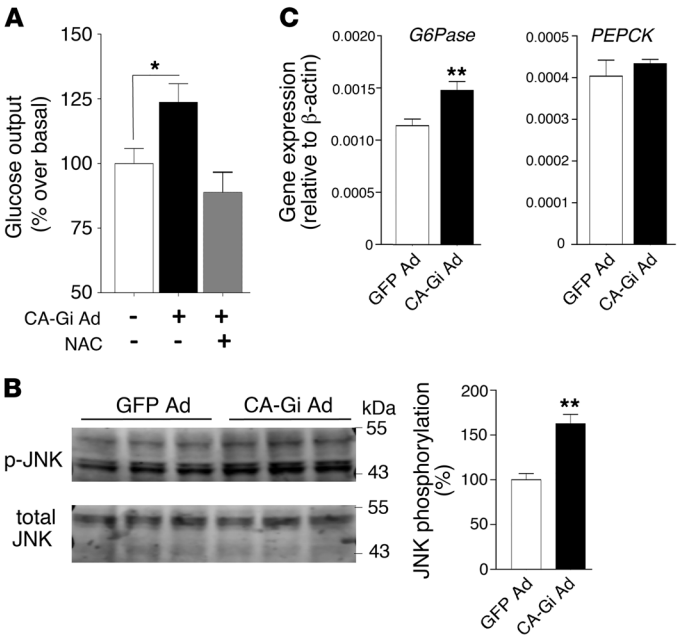

Figure 6. Studies with primary human hepatocytes. (**A**) Glucose output measurements. Primary human hepatocytes were transduced with an adenovirus coding for a constitutively active version of $G\alpha_{i2}$ (CA-Gi Ad) or a control adenovirus coding for GFP (GFP Ad). Cells expressing the CA-Gi construct showed a significant increase in glucose output. This effect was abolished in the presence of NAC (5 mM), a ROS scavenger. (**B**) Western blot and (**C**) gene expression analyses. Human hepatocytes infected with CA-Gi Ad showed increased p-JNK levels (**B**) and elevated *G6Pase* transcript levels (**C**). The graph in **B** summarizes all Western blot data. Data represent the mean ± SEM from 3 independent experiments. $^*P < 0.05$ and $^{**}P < 0.01$, compared with the corresponding control group. Statistical significance was determined by (**A**) 1-way ANOVA with a Benjamini-Hochberg correction and (**B** and **C**) 2-tailed Student's *t* test. See complete unedited blots in the supplemental material.

promote glucose release from Hep-Di hepatocytes (Supplemental Figure 6C). Thus, it is unlikely that Di-induced ERK phosphorylation contributes to the impairments in glucose homeostasis triggered by stimulation of hepatic G_i signaling.

Critical role of JNK activation in mediating Di-stimulated HGP. We found that CNO treatment (10 μM) of Hep-Di hepatocytes also led to a significant stimulation of JNK phosphorylation, in a PTX-sensitive manner (Figure 3B). Strikingly, CNO-induced stimulation of glucose release from Hep-Di hepatocytes, but not the corresponding glucagon response, could be totally blocked by BI87G3 (10 μM), a selective JNK inhibitor (Figure 3C). Consistent with these in vitro data, we observed that CNO treatment (10 mg/kg i.p.) of Hep-Di mice also resulted in a significant increase in hepatic JNK phosphorylation (Figure 3D).

To further confirm the importance of JNK signaling in Di-mediated hyperglycemic responses in vivo, we generated mice expressing a dominant-negative version of JNK (JNK-DN) selectively in hepatocytes of Hep-Di mice (Hep-Di-JNK–DN mice). These mice were generated by injecting an adenovirus coding for JNK-DN (34) into the tail vein of Hep-Di mice. A CNO challenge test showed that CNO-induced (10 mg/kg i.p.) increases in blood glucose levels were significantly reduced in Hep-Di-JNK–DN mice as compared with Hep-Di mice (Figure 3E), indicating that JNK activation plays a key role in mediating G_i-dependent hyperglycemic responses in vivo. CNO-induced blood glucose elevations were greatly reduced but not abolished in Hep-Di-JNK–DN mice (Figure 3E). One possible explanation for this finding is that other signaling pathways, besides the JNK cascade, contribute to G_i-mediated increases in HGP. Alternatively, it is possible that the JNK-DN construct was unable to suppress hepatic JNK signaling completely.

Activation of hepatic JNK signaling modulates the expression of genes regulating hepatic glucose fluxes, including *G6Pase* and *PEPCK*, the 2 rate-controlling enzymes in the process of gluconeogenesis. Consistent with this notion, CNO treatment (10 mg/kg i.p.) of Hep-Di mice increased the hepatic expression of these 2 key enzymes (Supplemental Figure 7A). Studies with isolated Hep-Di hepatocytes showed that selective inhibition of JNK by BI87G3 (10 μM) drastically reduced CNO-induced increases in *G6Pase* expression (Supplemental Figure 7B).

Since enhanced JNK activity has been linked to impaired insulin receptor signaling in various cell types (32, 35), we studied insulin-induced (10 nM) AKT and ERK phosphorylation in isolated Hep-Di hepatocytes, in the absence or presence of CNO (10 μM). Western blot studies demonstrated that insulin-mediated increases in AKT and ERK phosphorylation were not reduced upon costimulation of Hep-Di hepatocytes with CNO (Supplemental Figure 8). This observation strongly suggests that activation of G_i-type G proteins promotes hepatic glucose release independently of insulin receptor signaling.

Inhibition of the PI3K pathway does not affect Di-dependent activation of HGP. Since G_i signaling can also stimulate the PI3K pathway (36, 37), we studied the possible contribution of this pathway to Di-mediated increases in HGP. Specifically, we measured CNO-induced glucose output from Hep-Di hepatocytes in the absence or presence of LY294002 (20 μM), a selective PI3K inhibitor. We found that the presence of the PI3K inhibitor had no significant effect on CNO-induced glucose release (Supplemental Figure 9), suggesting that the PI3K pathway does not make a significant contribution to the Di-mediated increase in HGP.

Hepatocyte Di signaling promotes oxidative phosphorylation and ROS production. We designed a series of experiments to elucidate the pathway that links hepatic G_i signaling to JNK activation. JNKs are activated by various stress stimuli that produce ROS (38). In agreement with this notion, we found that CNO (10 μM) treatment of Hep-Di hepatocytes triggered pronounced increases in ROS production in a time-dependent and PTX-sensitive (300 ng/ml) fashion (Figure 4A), indicating that activation of G_i-type G proteins stimulates ROS accumulation in hepatocytes. Interestingly, pretreatment of Hep-Di hepatocytes with *N*-acetyl cysteine (NAC) (5 mM), a ROS scavenger, completely blocked CNO-induced (10 μM) JNK phosphorylation increases (Figure 4B).

We next hypothesized that Di-mediated ROS formation was triggered by an increase in the rate of mitochondrial oxidative phosphorylation (39). To address this question, we measured the CNO-induced oxygen consumption rate (OCR) of Hep-Di hepatocytes by using Seahorse technology. Strikingly, CNO (10 μM) treatment of Hep-Di hepatocytes (Figure 4C), but not of control hepatocytes (Figure 4D), strongly increased basal respiration in a PTX-sensitive fashion.

To further strengthen the link between Di-mediated increases in ROS production and enhanced HGP, we treated Hep-Di hepatocytes with the ROS scavenger NAC (5 mM), either in the absence or presence of CNO 10 μM) or glucagon (100 nM). Strikingly, we observed that the CNO-induced increase in glucose output, but not the corresponding glucagon response, was completely blocked in the presence of NAC (Figure 4E).

Taken together, these data indicate that activation of hepatic G_i signaling stimulates the OCR, resulting in increased ROS production and activation of JNK, which eventually stimulates HGP.

RNA-sequencing analysis of hepatic gene expression following CNO treatment of Hep-Di mice. While we demonstrated that intact JNK signaling is required for maximal glucose output after stimulation of hepatic G_i signaling, other pathways may also contribute to this response, as suggested by the data in Figure 3E. To obtain information about such non–JNK-dependent pathways, we studied changes in hepatic gene expression in an unbiased fashion using RNA-sequencing (RNA-seq) analysis. We prepared liver RNA from Hep-Di mice 30 minutes after injection with either CNO (10 mg/kg i.p.) or saline (control) and then subjected these RNA samples to RNA-seq analysis. Gene expression analysis showed that CNO treatment of Hep-Di mice led to the differential expression of more than 1,000 hepatic genes (Supplemental Figure 10 and Supplemental Table 3). Interestingly, many genes associated with increased ER stress and the linked unfolded protein response (UPR) were upregulated after activation of hepatic Di signaling (Supplemental Figure 10B). It is well known that ER stress and the resulting UPR promote ROS production and JNK activation (32, 40, 41), as observed in the present study. The CNO group also displayed altered expression levels of many genes involved in activation of the Nrf2/antioxidant response element signaling pathway, a major mechanism in the cellular defense against oxidative stress (Supplemental Figure 10B) (40). Stimulation of hepatic Di signaling also enhanced the expression of several genes involved in the p38/MAPK signaling pathway (Supplemental Figure 10B). This observation is of particular interest, since activation of p38 has been linked to elevated hepatic gluconeogenesis (42). On the basis of these results, it is likely that other cellular pathways, besides JNK-induced signaling, also contribute to the observed increases in G_i-mediated HGP. The precise nature and relative contribution of these additional, non-JNK pathways to the observed metabolic phenotypes will be the subject of future studies.

Activation of a G_i-coupled receptor endogenously expressed by hepatocytes. Hepatocytes express a number of endogenous G_i-coupled receptors including α_2-adrenergic (11) and CB_1 cannabinoid receptors (12, 13). Interestingly, recent studies have shown that mice lacking CB_1 receptors selectively in hepatocytes show significant improvements in glucose homeostasis in various metabolic assays (12, 13). Consistent with this observation, we found that injection of control mice with anandamide (AEA) (10 mg/kg i.p.), a cannabinoid receptor agonist, led to markedly impaired glucose tolerance (IGTT; Figure 5A). Importantly, this AEA effect was absent in Hep-Gi–KO mice (Figure 5B), strongly supporting the concept that AEA-induced glucose intolerance is caused by G_i signaling triggered by activated hepatic CB_1 receptors.

To demonstrate that hepatic CB_1 receptors were able to activate a signaling pathway similar to that of the Di designer receptor, we carried out additional functional assays with WT mouse hepatocytes. To increase CB_1 receptor expression levels, hepatocytes were obtained from mice that had been maintained on a HFD (13). As observed with CNO-treated Hep-Di hepatocytes, treatment of WT hepatocytes with a CB_1 receptor agonist (150 nM methanandamide [M-AEA]) caused a significant increase in glucose output (Figure 5, C and D). Strikingly, this response was completely absent in the presence of the ROS scavenger NAC (5 mM) or the selective JNK inhibitor BI87G3 (10 μM) (Figure 5, C and D, respectively). As expected, CB_1 receptor activation (agonist: HU210, 1 μM) caused significant, time-dependent increases in JNK phosphorylation (Figure 5, E and F) that were not observed in NAC-treated (5 mM) hepatocytes (Figure 5, E and F). Taken together, these data strongly support the concept that activation of endogenous hepatocyte CB_1 receptors, like stimulation of hepatic Di signaling, promotes ROS formation, resulting in the activation of JNK and enhanced hepatic glucose production.

Altered gene expression in livers prepared from fasted WT mice. We next examined hepatic gene expression levels in fasted WT mice. qRT-PCR studies showed that the hepatic expression levels of $G\alpha_{i1}$ and the G_i-coupled α_{2A}-adrenergic receptor were significantly increased in mice after a 16-hour fast (Supplemental Figure 11). These findings are consistent with the concept that enhanced hepatic G_i signaling plays a role in promoting HGP under physiological conditions.

G_i signaling stimulates glucose release in human hepatocytes. To study whether increased G_i signaling also led to enhanced HGP in human liver, we transduced human primary hepatocytes with an adenovirus coding for a constitutively active version of $G\alpha_{i2}$ (CA-Gi) (43). We found that human CA-Gi hepatocytes had a significant increase in glucose output (Figure 6A). This CA-Gi–dependent effect was abolished in the presence of NAC (5 mM), strongly suggesting that G_i stimulates HGP via a similar signaling pathway in mouse and human hepatocytes. Moreover, human CA-Gi hepatocytes showed significant increases in JNK phosphorylation and *G6Pase* transcript levels (Figure 6, B and C), consistent with the data obtained in mouse hepatocytes.

Altered gene expression in hepatic tissue from patients with nonalcoholic steatohepatitis. We also performed gene expression analyses using RNA prepared from the livers of patients with nonalcoholic steatohepatitis (NASH) and from healthy controls. Except for 1 individual, 14 of the 15 patients with NASH showed clear signs of insulin resistance (Supplemental Table 2). Consistent with this observation, NASH is known to be strongly correlated with hepatic insulin resistance (44, 45). Interestingly, qRT-PCR studies showed that the hepatic expression levels of the α_{2A}-adrenergic and CB_1 cannabinoid receptors, 2 prototypical G_i-coupled receptors expressed by hepatocytes (11–14), were greatly increased in NASH patients (Supplemental Figure 12). On the other hand, the hepatic RNA levels of $G\alpha_{i1}$ and $G\alpha_{i3}$ were significantly reduced in patients with NASH (Supplemental Figure 12), most likely because of counterregulatory mechanisms caused by enhanced G_i signaling through α_{2A}-adrenergic and CB_1 receptors and, perhaps, other G_i-coupled receptors.

Discussion

An increase in HGP is one of the key features of T2D (2–4). Previous studies have shown that enhanced hepatic glucagon/GCGR signaling greatly contributes to this metabolic deficit

(4, 7). Activated GCGRs couple to the stimulatory G protein G_s, which in turn activates adenylyl cyclase and PKA, ultimately triggering a series of signaling events that promote glycogen breakdown and gluconeogenesis (6).

In contrast to the GCGR and other G_s-coupled receptors, GPCRs that preferentially couple to G_i-type proteins are known to inhibit the function of adenylyl cyclase (10). We therefore tested the hypothesis that activation of hepatocyte G_i signaling might represent a new strategy to reduce pathologically enhanced GCGR activity. Hepatocytes express several G_i-linked receptors including α_2-adrenergic (11) and CB_1 cannabinoid receptors (12, 13). However, these receptors, like virtually all other nonsensory GPCRs, are expressed in many other tissues and cell types (14). For this reason, it is not possible to selectively stimulate native G_i-coupled receptors in hepatocytes by simply administering receptor-selective agonists in vivo. To circumvent this limitation, we took advantage of the availability of a new class of designer GPCRs known as DREADDs (15, 16, 46). Importantly, DREADDs do not bind any endogenous ligands but can be selectively activated by CNO, a synthetic drug that is otherwise pharmacologically inert (15, 16, 46).

In the present study, we used a viral delivery strategy to selectivity express Di, a G_i-coupled DREADD (15, 16), in mouse hepatocytes. In vitro studies with isolated hepatocytes demonstrated that CNO-mediated activation of Di signaling inhibited GCGR-mediated increases in cAMP levels (Supplemental Figure 2A), as expected for a G_i-coupled receptor. However, in contrast to our initial hypothesis, CNO treatment of isolated Di hepatocytes promoted HGP (Figure 3A). This effect was abolished in the presence of PTX (Figure 3A), indicating the involvement of G proteins of the G_i family.

In agreement with the in vitro studies, in vivo studies in both fed and fasted mice showed that activation of hepatic Di signaling caused pronounced increases in blood glucose levels, impaired glucose tolerance, and increased blood glucose excursions in a PTT (Figure 1, A–D). Moreover, the hyperglycemic effects of exogenously administered glucagon were further enhanced after treatment of Hep-Di mice with CNO (Figure 1F). Quantification of hepatic glucose fluxes in conscious Hep-Di mice revealed that CNO-mediated activation of hepatic G_i signaling resulted in significant increases in both the rate of glycogen breakdown and gluconeogenesis (Figure 1, I and J), indicating that both of these processes contribute to G_i-mediated stimulation of HGP in vivo.

By using a mouse model lacking functional G_i proteins selectively in hepatocytes, we demonstrated that the hyperglycemic effects mediated by activation of hepatic Di signaling indeed required functional G_i proteins (Figure 2A). Moreover, in vivo studies using an anti-GCGR antibody showed that the hyperglycemic effects caused by stimulation of hepatic Di signaling did not require the presence of functional GCGRs (Supplemental Figure 4).

Taken together, these observations strongly support the surprising concept that activation of hepatic G_i signaling does not inhibit HGP but rather stimulates glucose release from the liver. In agreement with this notion, we demonstrated that mice lacking functional G_i proteins selectively in hepatocytes (Hep-Gi–KO mice) had in vivo metabolic phenotypes that were opposite those observed after stimulation of hepatocyte G_i signaling in CNO-treated Hep-Di mice (Figure 2, B–E). Importantly, Hep-Gi–KO mice were protected against metabolic deficits caused by the consumption of a HFD (Figure 2, D and E). This observation suggests that suppression of hepatic G_i signaling may prove beneficial for restoring euglycemia in T2D.

We also delineated a cellular pathway that links G_i activation to enhanced HGP. We found that activation of hepatic G_i signaling promotes the production of ROS, which in turn leads to the activation of JNK, which ultimately triggers enhanced HGP and impaired glucose homeostasis (Figure 3 and Figure 4). CNO-activated G_i signaling greatly enhanced the hepatocyte OCR (Figure 4C), providing a potential mechanism for the observed G_i-mediated increase in ROS production.

It should be noted in this context that activation of chemoattractant GPCRs, including the fMLF and C5a receptors, also promotes ROS production in neutrophils in a G_i-dependent fashion (47). In these cells, ROS accumulation requires the activity of multiple signaling pathways including the activation of PI3 kinase and the small GTPase Rac (47). It remains to be explored whether similar signaling cascades are involved in G_i-mediated ROS production in hepatocytes.

In vitro studies showed that G_i-mediated increases in HGP were abolished by a selective JNK inhibitor (Figure 3C). Moreover, the CNO-mediated increases in blood glucose levels in Hep-Di mice were greatly reduced by the hepatocyte-specific expression of a DN version of JNK (Figure 3E). Taken together, these data strongly support the concept that activation of JNK plays a central role in the detrimental metabolic effects caused by hepatic G_i signaling.

Somewhat surprisingly, we observed that increased JNK activity did not lead to impaired insulin signaling in Hep-Di hepatocytes (Supplemental Figure 9), perhaps because of other compensatory cellular effects induced by the activation of G_i-linked receptors. However, in vivo and in vitro studies showed that activation of G_i signaling in Hep-Di hepatocytes led to a robust, JNK-dependent increase in the expression of *G6Pase* (Supplemental Figure 8). Consistent with these findings, a recent study demonstrated that JNK plays a key role in activating the *G6Pase* promoter in rodent primary hepatocytes, even in the absence of insulin receptor signaling (48). Taken together, these observations, in conjunction with the known central role of G6Pase in promoting HGP, suggest that the G_i/JNK/G6Pase pathway plays a major role in G_i-mediated hepatic glucose release. However, we cannot exclude the possibility that additional JNK-independent mechanisms contribute to the changes in glucose homeostasis observed after stimulation of hepatic G_i signaling in vivo.

Studies with primary human hepatocytes indicated that a similar pathway was also operative in human liver (Figure 6). Importantly, we found that primary human hepatocytes expressing a constitutively active version of $G\alpha_{i2}$ (CA-Gi) (43) had a significant increase in glucose output and that this effect could be blocked by a ROS scavenger (Figure 6A).

To demonstrate that our findings are also applicable to G_i-coupled receptors that are endogenously expressed by hepatocytes, we further analyzed signaling through hepatocyte CB_1 cannabinoid receptors (12, 13). Consistent with the outcome of a previous study (12), acute i.p. treatment of WT mice with AEA, a cannabinoid receptor agonist, caused severely impaired glucose tolerance (Figure 5A). This effect was completely abolished in

Hep-Gi–KO mice (Figure 5B), indicating that activation of hepatic G_i proteins by an endogenously expressed G_i-coupled receptor also led to deficits in glucose homeostasis in vivo.

We also showed that activation of hepatic CB_1 receptors led to enhanced glucose release from hepatocytes via a signaling pathway similar to that stimulated by the Di designer receptor (Figure 5). Thus, these data strongly support the notion that activation of G_i-coupled receptors endogenously expressed by hepatocytes promotes ROS formation, resulting in JNK activation and enhanced HGP.

In summary, we report the surprising finding that activation of hepatic G_i-type G proteins leads to an increase in HGP and a deterioration of glucose homeostasis. On the other hand, selective inactivation of G_i-type G proteins in hepatocytes results in the opposite phenotype of reduced HGP and improved glucose tolerance. We conclude that hepatic G_i signaling represents a physiologically relevant pathway that is critical for regulating whole-body glucose homeostasis and that agents able to suppress hepatocyte G_i signaling (e.g., antagonists of G_i-coupled receptors endogenously expressed by hepatocytes) may be useful as antidiabetic drugs.

Methods

Drugs. CNO was obtained from the NIH as part of the Rapid Access to Investigative Drug Program funded by the National Institute of Neurological Disorders and Stroke (Bethesda, Maryland, USA). [^{3}H]-NMS (85.4 Ci/mmol) was purchased from PerkinElmer Life Sciences. Insulin (human) was obtained from Eli Lilly (Humulin). AEA, R(+)–M-AEA, PTX, and HU210 were obtained from Tocris. LY294002 was purchased from Cell Signaling Technology. All other drugs used were obtained from MilliporeSigma (BI87G3, U0126, NAC, atropine sulfate, sodium pyruvate, sodium lactate, glucagon, antimycin A, and rotenone).

Mouse maintenance and diet. Mice were housed in a specific pathogen–free barrier facility and maintained on a 12-hour light/12-hour dark cycle (light period from 6:00 am to 6:00 pm). Mice were provided ad libitum access to water and consumed either standard mouse chow (4% [w/w] fat content; Zeigler) or a HFD (35.5% [w/w] fat content; F3282; Bio-Serv).

Recombinant AAVs. AAVs coding for Cre recombinase (AAV-TBG-CRE) or EGFP (AAV-TBG-EGFP), respectively, were obtained from the Vector Core of the University of Pennsylvania (Philadelphia, Pennsylvania, USA) (49). AAV-TBG-CRE directs the selective expression of Cre recombinase in hepatocytes (Cre expression is under the transcriptional control of the hepatocyte-selective thyroxine-binding globulin [*TBG*] promoter). The AAV-TBG-EGFP virus, which codes for EGFP, was used for control purposes. We also prepared an AAV construct, in which we inserted the Di (hM4Di) coding sequence into the AAV-TBG plasmid, yielding AAV-TBG-Di. Viral particles (serotype 8) were generated by the Vector Core of the University of Pennsylvania.

Generation of Hep-Di mice. In order to generate mice expressing the Di designer receptor selectivity in hepatocytes (Hep-Di mice), 8-week-old male WT C57BL/6J mice (Taconic) were injected with 1×10^{11} infectious particles of the AAV-TBG-Di virus. To generate a cohort of control mice, 8-week-old male WT C57BL/6J mice were injected in the same fashion with the AAV-TBG-EGFP control virus. AAVs were suspended in 100 μl saline and delivered via the tail vein.

Generation of Hep-Gi–KO mice. To selectively inactivate G_i-type G proteins in hepatocytes, we used mice expressing S1-PTX, a known inhibitor of $G_{i/o}$ signaling, under the control of the *ROSA26* locus in a Cre recombinase–dependent manner (*ROSA26^{PTX}* mice on a C57BL/6J genetic background) (24). In *ROSA26^{PTX}* mice, the coding sequence of S1-PTX is preceded by a floxed silencer cassette (24). To achieve selective expression of S1-PTX in hepatocytes, 8-week-old female *ROSA26^{PTX}* mice were injected with the AAV-TBG-CRE virus (1×10^{11} infectious units). To generate a group of control animals, 8-week-old female *ROSA26^{PTX}* mice were treated in the same manner with the AAV-TBG-EGFP control virus. Viruses were delivered via the tail vein suspended in 100 μl saline.

Generation of Hep-JNK–DN and Hep-Di-JNK–DN mice. To obtain Hep-Di mice expressing a DN version of JNK selectively in hepatocytes (Hep-Di-JNK–DN mice), we coinjected 8-week-old male WT C57BL/6 mice (Taconic) with the AAV-TBG-Di virus (1×10^{11} infectious units) and an adenovirus coding for a DN version of JNK (Ad-JNK–DN; 1.5×10^9 infectious units) (34). Using the same strategy, we generated Hep-JNK–DN mice by injecting the Ad-JNK–DN virus together with the AAV-TBG-EGFP control virus. Viruses were suspended in 100 μl saline and delivered via the tail vein.

cAMP assay. Primary mouse hepatocytes were suspended at a density of 2×10^6 cells per milliliter in phenol red–free William's medium containing 500 μM IBMX. Subsequently, 5-μl aliquots of the cell suspension were added to the wells of a white-bottomed, 384-well plate (~10,000 cells/well). Cells were then incubated for 25 minutes at 37°C in the presence of increasing concentrations of glucagon and a fixed concentration of CNO (10 μM). After this incubation step, cells were lysed, and changes in intracellular cAMP levels were determined by using a FRET-based cAMP Detection Kit (cAMP Dynamic 2 Kit; Cisbio) (50).

Calcium mobilization assay. Primary hepatocytes were plated at a density of 3.5×10^4 cells per well in collagen-coated, 96-well, black-walled, clear-bottomed plates (Thermo Scientific) in medium consisting of DMEM containing 10% FBS. Approximately 18 hours later, agonist-mediated changes in $[Ca^{2+}]_i$ levels were measured using FLIPR technology (Molecular Devices). Hepatocytes were exposed to increasing concentrations of CNO or AVP as described previously (51). Increases in $[Ca^{2+}]_i$ were expressed as changes in fluorescence (peak fluorescence activity minus basal fluorescence activity) divided by basal fluorescence levels. Agonist concentration-response curves were analyzed using GraphPad Prism 4.0 (GraphPad Software).

Radioligand binding studies. Radioligand binding studies were performed with membranes prepared from mouse liver tissue. Liver membranes were obtained as described in detail previously (52). Binding reactions containing approximately 10 μg membrane protein per tube were carried out for 2 hours at 22°C in 0.5 ml binding buffer containing 25 mM sodium phosphate and 5 mM $MgCl_2$ (pH 7.4). We used 6 different concentrations of the [^{3}H]-NMS radioligand, ranging from 1 to 40 nM. Nonspecific binding was defined as the binding observed in the presence of 10 μM atropine. Binding reactions were terminated by rapid filtration over GF/C Brandel filters, followed by 3 washes with ice-cold distilled water. The amount of radioactivity that remained bound to the filters was determined by liquid scintillation spectrometry. Saturation binding data were analyzed by using GraphPad Prism 4.0 software.

In vivo metabolic tests. Mouse phenotyping studies were initiated 2 weeks after treatment of mice with AAVs or 3 to 5 days after infection with adenoviruses. In vivo metabolic tests were performed with male or female mice (10–20 weeks of age) using standard procedures.

In brief, prior to IGTTs, mice were fasted overnight for approximately 12 hours. Blood glucose concentrations were determined using blood collected from the tail vein immediately before and at defined time points after i.p. injection of glucose (1 or 2 g/kg). For PTTs and ITTs, mice were fasted in the same fashion and then injected i.p. with either sodium pyruvate (2 g/kg) or human insulin (0.75 U/kg; Humulin; Eli Lilly), followed by the monitoring of blood glucose levels. To assess the sensitivity of mice to exogenously administered glucagon, glucagon challenge tests were performed using mice that had ad libitum access to food or had been fasted overnight for approximately 12 hours. Blood glucose levels were determined at various time points after i.p. injection of glucagon (16 μg/kg).

In some of the tests, the mice were injected with the anti-GCGR antibody mAb7.v44 (10 mg/kg i.p.; Genentech) (19) twenty-four hours prior to treatment with CNO (10 mg/kg i.p.) or glucagon (16 μg/kg).

To study glucose-stimulated insulin secretion (GSIS), male Hep-Di and control mice (10–20 weeks of age) were fasted overnight for approximately 12 hours and then coinjected with glucose and CNO (glucose, 2 g/kg; CNO, 10 mg/kg), followed by monitoring of plasma insulin levels.

Blood glucose levels were monitored using an automated blood glucose reader (Glucometer Elite Sensor; Bayer). Plasma insulin levels were determined using an ELISA kit (Crystal Chem Inc.), according to the manufacturer's instructions.

In vivo analysis of hepatic glucose fluxes. Male Hep-Di mice and control mice (~15 weeks of age) were generated by AAV injections as described in the *Generation of Hep-Di mice* section. Studies were initiated 2 weeks after viral treatment. Catheters were implanted under isoflurane anesthesia in the right jugular vein and left common carotid artery for infusion of tracers and sampling of blood, respectively (20, 53). Following the surgery, the animals were individually housed and their body weights recorded. Five days after surgery, on the day of the study, the mice were placed in bedded containers (at 7:00 am), and food was removed. Infusion lines were connected through a swivel system to the catheters of unrestrained, conscious mice to allow freedom of movement. At 10:00 am (t_{-150} min), a bolus of [6,6-D_2]-glucose (80 mg/kg) and D_2O (1.5 mg/kg) were given over a 40-minute period. This was followed by a constant infusion of [6,6-D_2]-glucose (0.8 mg/kg/min) diluted in saline containing 4.5% D_2O that was maintained for the duration of the study. At t_{-20} minutes and t_0 minutes, blood samples were taken to assess glucose concentrations and glucose enrichment. At t_0 minutes, a bolus of CNO (10 mg/kg) was given via the jugular vein catheter. Blood samples were taken every 10 minutes for 50 minutes. Reconstituted red blood cells from a donor mouse were continuously infused (4 μl/min) for the duration of the study.

Glucose isotopomer distribution in arterial plasma was determined in the Vanderbilt Hormone Assay and Analytical Services Core using Agilent 5977A MSD GC/MS (Agilent Technologies) according to the method of Antoniewicz et al. (54) and analyzed using isotopomer computational analysis software (55). Glucose fluxes were assessed using non–steady-state equations (volume of distribution of glucose= 130 ml/kg) (56, 57). The contribution of gluconeogenesis was assessed as the enrichment ratio of deuterium enrichment on the fifth carbon of glucose/deuterium enrichment on the second carbon of glucose (54, 58).

In vivo studies in AEA-treated mice. Adult female Hep-Gi–KO and control mice (at least 16 weeks of age) that had been fasted overnight for approximately 12 hours were injected with AEA (10 mg/kg i.p.), a cannabinoid receptor agonist. AEA was prepared in a saline/DMSO/Tween-80 solution at a ratio of 18:1:1 (12). Ten minutes after AEA treatment, IGTTs were performed as described in the *In vivo metabolic tests* section.

Isolation and culture of primary mouse hepatocytes. Mice (10- to 18-week-old males) were anesthetized with a single i.p. injection (250–500 mg/kg) of tribromoethanol (Avertin). Primary hepatocytes were then isolated using a 2-step collagenase perfusion protocol (59). Hepatocytes (~0.7×10^6 cells/well) were cultured at 60% to 70% confluence in DMEM (4.5 g/l glucose) containing 10% FBS in collagen I–coated, 6-well plates (Corning). Cells were then further processed for mitochondrial respiration or glucose production assays.

Glucose production studied with primary mouse hepatocytes. Primary mouse hepatocytes (~0.7×10^6 cells/well) were cultured in 6-well plates in medium (phenol red–free DMEM containing 10% FBS and 4.5 g/l glucose) for 4 to 6 hours at 37°C. The medium was then replaced with fresh phenol red–free DMEM containing 1 g/l glucose. Subsequently, hepatocytes were cultured overnight and then washed thoroughly with PBS. To stimulate glucose production, the medium was replaced with glucose- and phenol red–free DMEM supplemented with gluconeogenic substrates (20 mM sodium lactate and 2 mM sodium pyruvate, respectively) in the presence of glucagon (100 nM) or CNO (10 μM) and various inhibitors of distinct signaling pathways. Hepatocytes were incubated at 37°C for 4 hours, after which the culture medium was collected for the measurement of glucose concentrations using a glucose assay kit (MilliporeSigma). Hepatocytes were scraped off the wells with RIPA buffer containing a proteinase inhibitor cocktail from Roche in order to measure total protein per well using the bicinchoninic acid (BCA) method.

Mouse hepatocytes were also stimulated with M-AEA, a stable CB_1 receptor agonist. For this set of experiments, hepatocytes were isolated from WT mice that had been maintained on a HFD for 8 weeks (~12–16 weeks of age). Hepatocytes (~0.5×10^6 cells/well) were cultured overnight in 6-well plates in medium (phenol red–free DMEM containing 10% FBS and 4.5 g/l glucose) at 37°C. Hepatocytes were washed twice with PBS and then incubated with the JNK inhibitor BI87G3 (10 μM) or NAC (5 mM) for 2 hours (the DMSO concentration in the medium was kept at 1%) or were left untreated. Subsequently, hepatocytes were incubated at 37°C for 5 hours in the presence or absence of M-AEA (150 nM) and processed as described above.

Analysis of G_i-mediated glucose output from human hepatocytes. Human primary hepatocytes (Hum4113; Triangle Research Labs) were seeded into collagen I–coated 6-well plates (Corning) at a density of 0.8×10^6 cells per well (Human Hepatocyte Plating Medium; Triangle Research Labs). Six hours later, hepatocytes were transduced with an MOI of 10 (~10 viral particles/cell) of an adenovirus encoding a constitutively active version of $G\alpha_{i2}$ (CA-Gi) (43) in maintenance medium (Hepatocyte Maintenance Medium; Triangle Research Labs). Two hours later, the maintenance medium was replaced with fresh medium. On the next day, glucose output assays were carried out essentially as described in the *Hepatic glucose production studied with primary mouse hepatocytes* section. Hepatocytes were incubated with gluconeogenic substrates (20 mM sodium lactate and 2 mM sodium pyruvate, respectively) for 1 hour at 37°C.

Preparation of cDNA and qRT-PCR analysis. Using standard molecular techniques, cDNAs were prepared from mouse primary hepatocytes or other mouse tissues (cell types) for qRT-PCR studies (see Supplemental Table 1 for the primer sequences). Total mRNA was

extracted using an RNA kit from QIAGEN, following the manufacturer's protocol. qRT-PCR studies were conducted as described in detail previously (60). Gene expression data were normalized relative to the expression of β-actin.

Measurement of hepatocyte mitochondrial OCR. Measurements of hepatocyte respiration (OCR) were performed using the Seahorse XF24 Analyzer (Seahorse Bioscience). Primary hepatocytes from Hep-Di or control mice were plated at a density of 4×10^4 cells per well on collagen I–coated, 24-well Seahorse plates in complete media (phenol red–free DMEM containing 10% FBS and 4.5 g/l glucose), and the media were replaced approximately 6 hours later. On the following day, cells were pretreated with PTX (300 ng/ml) or vehicle for 2 hours. After 3 washes with Seahorse medium, OCR measurements were performed in Seahorse medium supplemented with 2 mM sodium pyruvate and 25 mM glucose, respectively (61). Hepatocytes were stimulated with 10 μM CNO in the presence or absence of PTX (300 ng/ml). Antimycin A and rotenone (5 μM each) were used to inhibit mitochondrial respiration. OCR data were normalized to the protein content per well.

Analysis of ROS production. Primary mouse hepatocytes were plated at a density of 3.5×10^4 cells per well in collagen-coated, 96-well, black-walled, clear-bottomed plates (Thermo Fisher Scientific) in DMEM containing 1 g/l glucose and 10% FBS, in the presence or absence of PTX (300 ng/ml). On the next day, CNO-induced (10 μM) increases in ROS production were measured using the OxiSelect Intracellular ROS Assay Kit (Cell Biolabs) and a Multimode Microplate Reader (Molecular Devices). Experiments were conducted according to the manufacturers' instructions. All reagents were dissolved in phenol red–free DMEM containing 1 g/l glucose. Increases in ROS accumulation were expressed as changes in fluorescence (peak fluorescence activity minus basal fluorescence activity). Data were analyzed using GraphPad Prism 4.0.

Western blot studies. Primary mouse hepatocytes were first cultured in 12-well plates for approximately 6 hours at 37°C in medium (phenol-free DMEM containing 10% FBS and 4.5 g/l glucose). The medium was then replaced with a fresh one, and hepatocytes were cultured overnight. On the next day, hepatocytes were thoroughly washed and treated with CNO (10 μM) and/or insulin (10 nM) at 37°C in a 5% CO_2 incubator. In a subset of experiments, cells were preincubated for 2 hours with PTX (300 ng/ml). Incubations were terminated with RIPA buffer containing protease and phosphatase inhibitor cocktails (Roche) at defined time points. Protein lysates were subjected to SDS-PAGE after denaturation of proteins at 95°C. Immunoblot studies were performed using standard procedures (~10 μg protein/lane). Immunoreactive proteins were visualized using SuperSignal West Pico Chemiluminescent Substrate (Pierce, Thermo Fisher Scientific).

We also prepared liver lysates from mice that had been injected with CNO (10 mg/kg i.p.) or vehicle after a 4- to 5-hour fast. Mice were sacrificed 15 minutes after injections. Protein lysates were then subjected to Western blot analysis as described above. The following antibodies, all from Cell Signaling Technology, were used: phosphorylated JNK (p-SAPK/JNK [Thr183/Tyr185], rabbit mAb 4668; 1:1,000 dilution); total JNK (SAPK/JNK antibody 9252; 1:1,000 dilution); p-ERK (p-p44/42 MAPK [Thr202/Tyr204], rabbit mAb 4376; 1:1,000 dilution); total ERK (p44/p42 MAPK, ERK1/2 antibody 9102; 1:1,000 dilution); p-AKT (Ser473) (9271; 1:1,000 dilution); and total AKT (9272; 1:1,000 dilution).

Preparation of human liver RNA and gene expression analysis. Percutaneous liver biopsies of adult noncirrhotic NASH patients (n = 15) were obtained as described previously (62, 63) (for more detailed patient data, see Supplemental Table 2). Control liver biopsies were obtained from 5 nondiabetic patients (mean age, 47 years; n = 3 female patients) who had a past history of chronic hepatitis C and were successfully treated with viral eradication at least 6 months prior to the biopsy (64). Histological evaluation of these samples revealed no signs of steatosis or hepatic inflammation or injury.

A 2- to 5-mm sample from the liver biopsy specimen was flash-frozen at the bedside and archived at –80°C. For analysis, samples were homogenized in TRIzol (Invitrogen, Thermo Fisher Scientific), and total RNA was extracted according to the manufacturer's instructions. cDNA was synthesized using the First-Strand cDNA Synthesis System for Quantitative RT-PCR (OriGene), according to the manufacturer's protocol. Gene expression levels were measured by monitoring SYBR green fluorescence intensity over time using a CFX384 Touch Real-Time PCR System (Bio-Rad). Each PCR reaction (15 μl final volume) consisted of cDNA (15 ng), 7.5 μl of 2× SYBR Green PCR Master Mix (Applied Biosystems), and 100 nM of each PCR primer. For each primer pair, qRT-PCR reactions were performed in triplicate using a 384-well plate format. PCR cycling conditions were as follows: 95°C for 10 minutes, 40 cycles at 95°C for 15 seconds, and 60°C for 1 minute, respectively. The expression of β-actin (*ACTB*) served as an internal control.

Statistics. All data are expressed as the mean ± SEM. Prior to applying specific statistical tests, we performed tests for normality and homogeneity of variance. Data were then tested for statistical significance by 1- or 2-way ANOVA, followed by the post-hoc tests indicated in the figure legends, or by a 2-tailed, unpaired Student's t test, as appropriate. A P value of less than 0.05 was considered significant.

Study approval. All animal studies were approved by the IACUC of the NIDDK, NIH. Studies in humans were approved by the IRB of the NIDDK/NIAMS, and all subjects provided written informed consent.

Author contributions

MR, LZ, OPM, and JW designed and conceived the experiments. MR, LZ, SMM, SPP, SJ, LW, YC, RJL, AHC, YM, YR, and OPM performed and analyzed the experiments. HK prepared the Ad-JNK–DN virus. MJB provided novel reagents and helpful advice throughout the study. TJC and OPM performed and analyzed the hepatic glucose flux studies. JL and TF supervised and interpreted the OCR experiments. YM and YR generated and provided the human liver cDNA samples. MR, LZ, and JW wrote the manuscript.

Acknowledgments

This research was funded by the Intramural Research Program of the NIDDK, NIH and by NIDDK grant DK-043748 (to OPM). TJC was supported by NIDDK grant T32-DK-007563. The Vanderbilt Mouse Metabolic Phenotyping Center (NIDDK grant DK-59637) and the Hormone Assay and Analytical Services Core (NIDDK grants DK-059637 and DK-020593) provided surgical and analytical support, respectively. Harold Smith and his coworkers at the NIDDK Genomic Core provided expert support with the RNA-seq work. We thank Shaun R. Coughlin (UCSF, San Francisco, California, USA) for sending us a breeding pair of *ROSA26*^{PTX} mice. We also thank John Spouge (Head of the Statistical Computational Biology Group, NLM-NCBI, Bethesda, Maryland, USA) for his expert advice regarding the statistical analysis of our data. The Hum4113 cells were provided by Haiming Cao (NHLBI, NIH). The

CA-Gi adenovirus was provided by Kevin Donahue (University of Massachusetts Medical School, Worcester, Massachusetts, USA). The adenovirus coding for GFP (Ad-GFP) was a gift of the laboratory of Marc Montminy (Salk Institute for Biological Studies, La Jolla, California, USA).

Address correspondence to: Jürgen Wess, Laboratory of Bioorganic Chemistry, Molecular Signaling Section, National Institute of Diabetes and Digestive and Kidney Diseases, Building 8A, Room B1A-05, 8 Center Drive, Bethesda, Maryland 20892, USA. Phone: 301.402.3589; Email: jurgenw@niddk.nih.gov.

1. Lam DW, LeRoith D. The worldwide diabetes epidemic. *Curr Opin Endocrinol Diabetes Obes*. 2012;19(2):93–96.
2. Postic C, Dentin R, Girard J. Role of the liver in the control of carbohydrate and lipid homeostasis. *Diabetes Metab*. 2004;30(5):398–408.
3. Lin HV, Accili D. Hormonal regulation of hepatic glucose production in health and disease. *Cell Metab*. 2011;14(1):9–19.
4. Unger RH, Cherrington AD. Glucagonocentric restructuring of diabetes: a pathophysiologic and therapeutic makeover. *J Clin Invest*. 2012;122(1):4–12.
5. Exton JH. Mechanisms of hormonal regulation of hepatic glucose metabolism. *Diabetes Metab Rev*. 1987;3(1):163–183.
6. Estall JL, Drucker DJ. Glucagon and glucagon-like peptide receptors as drug targets. *Curr Pharm Des*. 2006;12(14):1731–1750.
7. Jiang G, Zhang BB. Glucagon and regulation of glucose metabolism. *Am J Physiol Endocrinol Metab*. 2003;284(4):E671–E678.
8. D'Alessio D. The role of dysregulated glucagon secretion in type 2 diabetes. *Diabetes Obes Metab*. 2011;13 Suppl 1:126–132.
9. Cho YM, Merchant CE, Kieffer TJ. Targeting the glucagon receptor family for diabetes and obesity therapy. *Pharmacol Ther*. 2012;135(3):247–278.
10. Pierce KL, Premont RT, Lefkowitz RJ. Seven-transmembrane receptors. *Nat Rev Mol Cell Biol*. 2002;3(9):639–650.
11. Exton JH. Mechanisms involved in alpha-adrenergic phenomena. *Am J Physiol*. 1985;248(6 Pt 1):E633–E647.
12. Liu J, et al. Hepatic cannabinoid receptor-1 mediates diet-induced insulin resistance via inhibition of insulin signaling and clearance in mice. *Gastroenterology*. 2012;142(5):1218–1228.e1.
13. Osei-Hyiaman D, et al. Hepatic CB1 receptor is required for development of diet-induced steatosis, dyslipidemia, and insulin and leptin resistance in mice. *J Clin Invest*. 2008;118(9):3160–3169.
14. Regard JB, Sato IT, Coughlin SR. Anatomical profiling of G protein-coupled receptor expression. *Cell*. 2008;135(3):561–571.
15. Armbruster BN, Li X, Pausch MH, Herlitze S, Roth BL. Evolving the lock to fit the key to create a family of G protein-coupled receptors potently activated by an inert ligand. *Proc Natl Acad Sci U S A*. 2007;104(12):5163–5168.
16. Rogan SC, Roth BL. Remote control of neuronal signaling. *Pharmacol Rev*. 2011;63(2):291–315.
17. Guettier JM, et al. A chemical-genetic approach to study G protein regulation of beta cell function in vivo. *Proc Natl Acad Sci U S A*. 2009;106(45):19197–19202.
18. Li JH, et al. A novel experimental strategy to assess the metabolic effects of selective activation of a G(q)-coupled receptor in hepatocytes in vivo. *Endocrinology*. 2013;154(10):3539–3551.
19. Mukund S, et al. Inhibitory mechanism of an allosteric antibody targeting the glucagon receptor. *J Biol Chem*. 2013;288(50):36168–36178.
20. Ayala JE, Bracy DP, McGuinness OP, Wasserman DH. Considerations in the design of hyperinsulinemic-euglycemic clamps in the conscious mouse. *Diabetes*. 2006;55(2):390–397.
21. Ayala JE, et al. Standard operating procedures for describing and performing metabolic tests of glucose homeostasis in mice. *Dis Model Mech*. 2010;3(9-10):525–534.
22. Ayala JE, et al. Hyperinsulinemic-euglycemic clamps in conscious, unrestrained mice. *J Vis Exp*. 2011;(57):3188.
23. Hasenour CM, et al. Mass spectrometry-based microassay of (2)H and (13)C plasma glucose labeling to quantify liver metabolic fluxes in vivo. *Am J Physiol Endocrinol Metab*. 2015;309(2):E191–E203.
24. Regard JB, et al. Probing cell type-specific functions of Gi in vivo identifies GPCR regulators of insulin secretion. *J Clin Invest*. 2007;117(12):4034–4043.
25. Pace AM, Faure M, Bourne HR. Gi2-mediated activation of the MAP kinase cascade. *Mol Biol Cell*. 1995;6(12):1685–1695.
26. O'Hayre M, Degese MS, Gutkind JS. Novel insights into G protein and G protein-coupled receptor signaling in cancer. *Curr Opin Cell Biol*. 2014;27:126–135.
27. Marinissen MJ, Gutkind JS. G-protein-coupled receptors and signaling networks: emerging paradigms. *Trends Pharmacol Sci*. 2001;22(7):368–376.
28. He JC, Neves SR, Jordan JD, Iyengar R. Role of the Go/i signaling network in the regulation of neurite outgrowth. *Can J Physiol Pharmacol*. 2006;84(7):687–694.
29. Pal M, Febbraio MA, Lancaster GI. The roles of c-Jun NH2-terminal kinases (JNKs) in obesity and insulin resistance. *J Physiol (Lond)*. 2016;594(2):267–279.
30. Liu Z, Cao W. p38 mitogen-activated protein kinase: a critical node linking insulin resistance and cardiovascular diseases in type 2 diabetes mellitus. *Endocr Metab Immune Disord Drug Targets*. 2009;9(1):38–46.
31. Tanti JF, Jager J. Cellular mechanisms of insulin resistance: role of stress-regulated serine kinases and insulin receptor substrates (IRS) serine phosphorylation. *Curr Opin Pharmacol*. 2009;9(6):753–762.
32. Vallerie SN, Hotamisligil GS. The role of JNK proteins in metabolism. *Sci Transl Med*. 2010;2(60):60rv5.
33. Seki E, Brenner DA, Karin M. A liver full of JNK: signaling in regulation of cell function and disease pathogenesis, and clinical approaches. *Gastroenterology*. 2012;143(2):307–320.
34. Nakatani Y, et al. Modulation of the JNK pathway in liver affects insulin resistance status. *J Biol Chem*. 2004;279(44):45803–45809.
35. Boucher J, Kleinridders A, Kahn CR. Insulin receptor signaling in normal and insulin-resistant states. *Cold Spring Harb Perspect Biol*. 2014;6(1):a009191.
36. Banquet S, et al. Role of G(i/o)-Src kinase-PI3K/Akt pathway and caveolin-1 in β_2-adrenoceptor coupling to endothelial NO synthase in mouse pulmonary artery. *Cell Signal*. 2011;23(7):1136–1143.
37. Lova P, et al. A selective role for phosphatidylinositol 3,4,5-trisphosphate in the Gi-dependent activation of platelet Rap1B. *J Biol Chem*. 2003;278(1):131–138.
38. Ip YT, Davis RJ. Signal transduction by the c-Jun N-terminal kinase (JNK)--from inflammation to development. *Curr Opin Cell Biol*. 1998;10(2):205–219.
39. Finkel T. Signal transduction by reactive oxygen species. *J Cell Biol*. 2011;194(1):7–15.
40. Cao SS, Kaufman RJ. Endoplasmic reticulum stress and oxidative stress in cell fate decision and human disease. *Antioxid Redox Signal*. 2014;21(3):396–413.
41. Hotamisligil GS. Endoplasmic reticulum stress and the inflammatory basis of metabolic disease. *Cell*. 2010;140(6):900–917.
42. Cao W, et al. p38 Mitogen-activated protein kinase plays a stimulatory role in hepatic gluconeogenesis. *J Biol Chem*. 2005;280(52):42731–42737.
43. Bauer A, et al. Inhibitory G protein overexpression provides physiologically relevant heart rate control in persistent atrial fibrillation. *Circulation*. 2004;110(19):3115–3120.
44. Postic C, Girard J. Contribution of de novo fatty acid synthesis to hepatic steatosis and insulin resistance: lessons from genetically engineered mice. *J Clin Invest*. 2008;118(3):829–838.
45. Chitturi S, et al. NASH and insulin resistance: Insulin hypersecretion and specific association with the insulin resistance syndrome. *Hepatology*. 2002;35(2):373–379.
46. Wess J, Nakajima K, Jain S. Novel designer receptors to probe GPCR signaling and physiology. *Trends Pharmacol Sci*. 2013;34(7):385–392.
47. Sun L, Ye RD. Role of G protein-coupled receptors in inflammation. *Acta Pharmacol Sin*. 2012;33(3):342–350.
48. Wang D, Wei Y, Schmoll D, Maclean KN, Pagliassotti MJ. Endoplasmic reticulum stress increases glucose-6-phosphatase and glucose cycling in liver cells. *Endocrinology*. 2006;147(1):350–358.
49. Miller RA, et al. Adiponectin suppresses gluconeogenic gene expression in mouse hepatocytes independent of LKB1-AMPK signaling. *J Clin Invest*. 2011;121(6):2518–2528.
50. Nakajima K, Wess J. Design and functional characterization of a novel, arrestin-biased designer G protein-coupled receptor. *Mol Pharmacol*. 2012;82(4):575–582.

51. Rossi M, et al. CK2 acts as a potent negative regulator of receptor-mediated insulin release in vitro and in vivo. *Proc Natl Acad Sci U S A*. 2015;112(49):E6818–E6824.
52. Li JH, et al. Hepatic muscarinic acetylcholine receptors are not critically involved in maintaining glucose homeostasis in mice. *Diabetes*. 2009;58(12):2776–2787.
53. Niswender KD, Shiota M, Postic C, Cherrington AD, Magnuson MA. Effects of increased glucokinase gene copy number on glucose homeostasis and hepatic glucose metabolism. *J Biol Chem*. 1997;272(36):22570–22575.
54. Antoniewicz MR, Kelleher JK, Stephanopoulos G. Measuring deuterium enrichment of glucose hydrogen atoms by gas chromatography/mass spectrometry. *Anal Chem*. 2011;83(8):3211–3216.
55. Young JD. INCA: a computational platform for isotopically non-stationary metabolic flux analysis. *Bioinformatics*. 2014;30(9):1333–1335.
56. Steele R, Wall JS, De Bodo RC, Altszuler N. Measurement of size and turnover rate of body glucose pool by the isotope dilution method. *Am J Physiol*. 1956;187(1):15–24.
57. Wall JS, Steele R, De Bodo RC, Altszuler N. Effect of insulin on utilization and production of circulating glucose. *Am J Physiol*. 1957;189(1):43–50.
58. Burgess SC, et al. Impaired tricarboxylic acid cycle activity in mouse livers lacking cytosolic phosphoenolpyruvate carboxykinase. *J Biol Chem*. 2004;279(47):48941–48949.
59. Li P, et al. A liver-enriched long non-coding RNA, lncLSTR, regulates systemic lipid metabolism in mice. *Cell Metab*. 2015;21(3):455–467.
60. Jain S, Ruiz de Azua I, Lu H, White MF, Guettier JM, Wess J. Chronic activation of a designer G(q)-coupled receptor improves β cell function. *J Clin Invest*. 2013;123(4):1750–1762.
61. Ho L, et al. SIRT4 regulates ATP homeostasis and mediates a retrograde signaling via AMPK. *Aging (Albany NY)*. 2013;5(11):835–849.
62. Loomba R, et al. Clinical trial: pilot study of metformin for the treatment of non-alcoholic steatohepatitis. *Aliment Pharmacol Ther*. 2009;29(2):172–182.
63. Promrat K, et al. A pilot study of pioglitazone treatment for nonalcoholic steatohepatitis. *Hepatology*. 2004;39(1):188–196.
64. Rotman Y, et al. Effect of ribavirin on viral kinetics and liver gene expression in chronic hepatitis C. *Gut*. 2014;63(1):161–169.